Electronic, Energetic, and Chemical Effects of Intrinsic Defects and Fe-Doping of $CoAl_2O_4$: A DFT+*U* Study

Aron Walsh,* Yanfa Yan, M. M. Al-Jassim, and Su-Huai Wei

National Renewable Energy Laboratory, Golden, Colorado 80401

Received: December 7, 2007; Revised Manuscript Received: April 16, 2008

The spinel cobalt aluminate has gained interest as a potential photoelectrochemical catalyst for the renewable production of hydrogen. Using band structure theory, we determine the energetics of possible intrinsic point defects in spinel $CoAl_2O_4$ and analyze their effect on its electronic and chemical properties. Extrinsic Fe-doping is also examined. Cation vacancies are found to be shallow acceptors, but their formation energy is sensitive to the growth conditions; an oxygen rich environment is required to enhance the p-type conductivity. Fe is an isovalent substituent on the Co (Al) site, exhibiting a preference for octahedral coordination, and forms a deep donor (acceptor) level near the center of the band gap, corresponding to a Fe(II) to Fe(III) transition.

1. Introduction

Building on the photoelectric effect discovered by Becquerel,[1,2] photoelectrochemical (PEC) splitting of H_2O is the most promising approach for renewable and efficient generation of hydrogen.[3,4] Despite the demonstration of the decomposition of water by TiO_2 in the 1970s,[5,6] progress in the subsequent three decades has been limited, and no materials have exhibited sustained efficiency. This is largely due to the numerous criteria, which should be satisfied by a candidate PEC catalyst: (i) band edges that bridge the water redox potential, (ii) a band gap of between 1.5 and 2 eV, (iii) strong absorption of visible light, (iv) good stability in aqueous media, (v) fast and efficient charge transfer to the electrolyte. Much attention has focused on metal oxides due to their high stability in electrolyte solutions and ease of production, but they are generally limited by too large band gaps (TiO_2, ZnO, WO_3) or too poor semiconducting properties (Fe_2O_3), which results in low device efficiencies under visible irradiation. An illustration of the principle PEC redox reactions for water splitting is shown in Figure 1. For a p-type photocatalyst, the photogenerated minority carriers (electrons) are injected into the electrolyte, driving the cathodic reduction of H^+ to form H_2. The generated majority carriers (holes) are injected into the counter electrode to forward the anodic oxidation of O^{2-} to O_2. For an n-type photocatalyst, the inverse charge transfer process occurs.

Ab initio design of novel PEC materials remains challenging due to the requirements outlined above. The approach we follow is to perform predictive simulations in unison with experiment. High-throughput-screening is an effective way of sifting through the many thousands of potential binary, ternary and quaternary metal oxide candidates. Woodhouse and Parkinson[7,8] have developed such an approach and reported encouraging behavior for the Co−Fe−Al oxide spinel system: a strong p-type photocurrent and an optical gap of ∼1.7 eV. Initially we analyzed the electronic properties of nine stoichiometric Co, Fe and Al containing spinels to narrow down the active composition, and identified $CoAl_2O_4$ as the most likely base material for PEC applications.[9] However, its optical gap of around 2 eV is larger than the 1.7 eV observed for the active material. In addition, while their material has been found to be Co and Al rich, when the Fe precursor is not included, the photogenerated current decreases, and thus far the nature of its contribution is unknown.

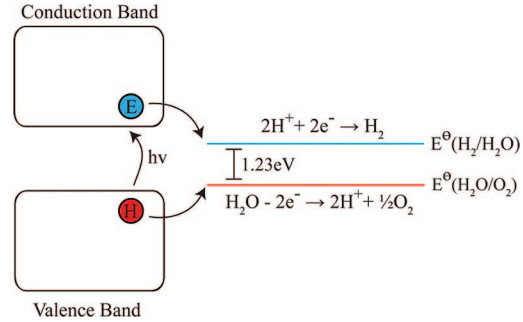

Figure 1. Schematic processes occurring in a p−n photoelectrochemical water splitting cell. Electrons and holes are indicated by the blue and red spheres, respectively.

In this paper we report an electronic structure study of intrinsic defects and Fe-doping of spinel $CoAl_2O_4$. Our principle aim is to answer two questions: (i) What defects are likely to contribute to p-type conductivity? (ii) What is the role of Fe in this system? Such an understanding will help direct further experimental endeavors to optimize this material and related potential catalysts. Using density functional theory (DFT), with the Co and Fe 3d states treated with on-site correction for Coulomb interactions (DFT+*U*), we examine nine point defects in the $CoAl_2O_4$ lattice (V_{Co}, V_{Al}, O_i, V_O, Co_{Al}, Al_{Co}), including local cation site disorder [Co_{Al}, Al_{Co}] and extrinsic Fe substitution (Fe_{Co}, Fe_{Al}). The calculated defect formation energies are related to experimentally accessible growth conditions via the introduction of equilibrium chemical potentials.

2. Properties of $CoAl_2O_4$

$CoAl_2O_4$ has been utilized as a ceramic pigment[10] (Thénard's blue) since the late 18th century and, in addition to optical coatings, is also important as a heterogeneous catalyst in the reformation of methane.[11] Like many other AB_2O_4 ternary

* To whom correspondence should be addressed. E-mail: aron_walsh@nrel.gov.

10.1021/jp711566k CCC: $40.75
Published on Web 07/11/2008

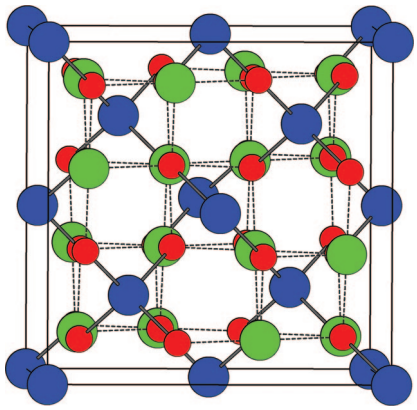

Figure 2. Cubic spinel structure of $CoAl_2O_4$. The Co atoms (blue) occupy tetrahedral sites and the Al atoms (green) occupy octahedral sites within an fcc oxygen sublattice (red).

oxides, $CoAl_2O_4$ adopts the spinel structure (space group $Fd\bar{3}m$) as shown in Figure 2. The lattice is based on a face centered cubic packing of oxygen atoms (32 e sites) and contains two distinct cation coordination sites. The Co(II) ions occupy 1/8 of the tetrahedral holes (8 a sites), while the Al(III) ions occupy 1/2 the available octahedral holes (16 d sites). Disorder in the cation distribution results in many of the interesting properties associated with spinel oxides[12–20] however, stoichiometric $CoAl_2O_4$ is known to be close to ideal at standard temperatures and pressures.[21,22] We have previously calculated the inversion energy (the cost of switching half-the Al and Co sites, forming the inverse spinel structure) as 0.52 eV per formula unit, which implies a cation inversion parameter of 0.07 at a formation temperature of 1000 K.[9]

The influence of the local T_d crystal field splits the Co 3d states into lower e_g and upper t_{2g} bands. The d^7 electronic configuration results in an $e_g^{2\uparrow}e_g^{2\downarrow}t_{2g}^{3\downarrow}$ arrangement, producing a local Co magnetic moment of 3 μ_B. No long-range magnetic ordering is observed down to temperatures as low as 2 K.[23] In contrast to the majority of metal oxides that are n-type through anion deficiency (e.g., ZnO, SnO_2, In_2O_3), $CoAl_2O_4$ exhibits hole mediated p-type conductivity,[24] as is characteristic of oxides formed from transition metals with accessible higher oxidation states. While the reported electronic conductivity of the stoichiometric bulk material has been low,[24] thin films of $CoAl_2O_4$ have been found to act as an effective electrode material.[25]

The solid state reaction of Co and Al oxides to form $CoAl_2O_4$ requires temperatures as high as 1200 °C.[26] However, when formed, $CoAl_2O_4$ is known to exhibit high chemical stability and is insoluble even in acidic solutions, which makes it particularly enticing for PEC applications. Interestingly, when initially prepared, samples of $CoAl_2O_4$ exhibit a green hue, while annealing at temperatures up to 1000 °C for 12 h is needed to obtain the distinctive deep color of Thénard's blue.[26–28] When excess Al precursors are used, this blue color is achieved more readily. UV−vis absorption measurements of $CoAl_2O_4$ indicate that the onset of optical absorption occurs from around 2 eV, with shifts observed depending on the preparatory conditions and annealing temperatures.[28]

3. Computational Methodology

Calculations on a 56 atom cubic spinel supercell were performed using DFT[29,30] as implemented in the VASP code.[31,32] A plane-wave basis set with a 500 eV upper energy threshold was employed, with a 5 × 5 × 5 special k-point grid[33] for Brillouin zone integration. The projector-augmented-wave method[34,35] was used to treat the valence-core interactions (Co, Fe:[Ar]; Al:[Ne]; O:[He]). To account for the correlated 3d orbitals of Fe and Co, the calculations were performed at the DFT+U level[36,37] using the PBE gradient corrected exchange−correlation functional.[38] $U - J = 2$ eV for Co 3d and $U - J =$ 3 eV for Fe 3d were chosen, as implemented in our previous study.[9] Unlike d^{10} oxides such as ZnO,[39] or highly correlated systems such as MgO:Li[40] and reduced TiO_2,[41] $CoAl_2O_4$ exhibits a very sensitive dependence to the application of U, as both the valence band maximum (VBM) and conduction band minimum (CBM) are of relatively localized Co 3d character. The application of $U - J = 2$ eV to Co 3d results in a band gap of 2.3 eV, reasonably consistent with experiment.[28]

The cell lattice vectors and atomic positions of $CoAl_2O_4$ were fully relaxed without constraint so that the force on all atoms remained within 5 meV/Å. The cell parameter of $a = 8.194$ Å was obtained from a fit to the Murnaghan equation of state,[42] which is within 1% of X-ray diffraction data.[43] The equilibrium cation−anion interatomic distances in the bulk solid were determined as R(Co−O) = 1.98 Å and R(Al−O) = 1.94 Å. For treatment of point defects, the cell volume is held constant, but the internal coordinates are fully relaxed for each configuration. For charged systems, a compensating homogeneous jellium background charge is assumed to preserve overall neutrality.

4. Defect Methodology

4.1. Formation Enthalpy of Neutral Defects. Our approach to modeling point defects follows the formalism adopted by Wei,[44] which has been successfully applied to a range of systems.[45–49] The formation enthalpy of a neutral defect can be obtained from

$$\Delta H_f^{\text{neutral}} = (E_{\text{Defect}} - E_{\text{Bulk}}) + \sum_i n_i E_i + n_i \mu_i \qquad (1)$$

where E_{Bulk} is the total energy of the bulk host lattice and E_{Defect} is the total energy of the defective cell. The elemental energies (E_i) are obtained from calculations of the constituent elements in their standard states using an equivalent basis set, i.e. bulk Fe, Co and Al metals, and an O_2 molecule. The chemical potentials of each constituent species (μ_i) can be varied to reflect specific equilibrium growth conditions, but are always globally constrained by the calculated formation enthalpy of $CoAl_2O_4$ in order to maintain the stability of the host:

$$\mu_{\text{Co}} + 2\mu_{\text{Al}} + 4\mu_{\text{O}} = \Delta H_f^{\text{CoAl}_2\text{O}_4} = -17.56 \text{ eV} \qquad (2)$$

4.2. Thermodynamic Limits on the Chemical Potentials. In addition to the host condition (eq 2), to avoid solid/gas elemental precipitation:

$$\mu_{\text{Co}} \le 0, \quad \mu_{\text{Al}} \le 0, \quad \mu_{\text{Fe}} \le 0, \quad \mu_{\text{O}} \le 0 \qquad (3)$$

Constraints are also imposed by the calculated formation enthalpies of the competing binary oxides of Co, Al and Fe to avoid the formation of alternative phases; for example,

$$3\mu_{\text{Co}} + 4\mu_{\text{O}} \le \Delta H_f^{\text{Co}_3\text{O}_4} = -8.48 \text{ eV} \qquad (4)$$

The resulting accessible range of the chemical potentials is illustrated in Figure 3 in a two-dimensional (μ_{Co}, μ_{Al}) plane. The vertices of the stability triangle are formed from the host condition (eq 2) giving the limits of Co/Al rich, Co poor and Al poor environments, respectively. From the constraints imposed by the competing binary oxides, the stable range of (μ_{Co}, μ_{Al}) for $CoAl_2O_4$ is shaded gray. Within this boundary, we explicitly consider two environments, one for cobalt rich

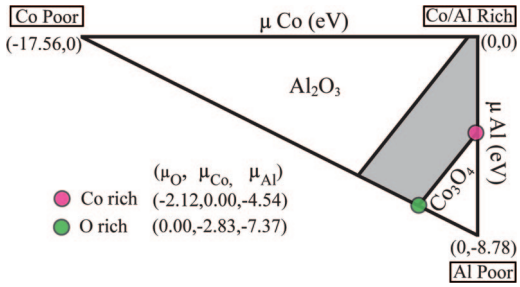

Figure 3. Illustration of the accessible (μ_{Co}, μ_{Al}) chemical potential range. The triangle vertices are determined by the formation enthalpy of $CoAl_2O_4$. Limits imposed by the formation of competing binary oxides result in the stable region shaded gray. The chosen Co and O rich environments are indicated by the red and green spheres, respectively.

(oxygen poor) conditions ($\mu_{Co} = 0$ eV), which results in $\mu_{Al} = -4.54$ eV, $\mu_O = -2.12$ eV. This region is most likely to correspond to the actual experimental conditions that the photoactive material was synthesized, where Co_3O_4 is a highly competitive phase, resulting in relatively poor Al conditions (the stabilization of defects that require the removal of Al from the system). We also consider alternative oxygen rich (metal poor) conditions,($\mu_O = 0$ eV), which result in $\mu_{Co} = -2.83$ eV, $\mu_{Al} = -7.37$ eV. This environment may be approached through appropriate choice of precursors or synthesizing at lower than ideal temperatures, where the stoichiometry of the lattice will be less than ideal. In the case of Fe-doping, the chosen oxygen chemical potentials result in $\mu_{Fe} = -1.00$ and -3.88 eV under Co and O rich environments, respectively.

4.3. Formation Enthalpy of Charged Defects. For treatment of defects in charge state q, the formation enthalpies are obtained from

$$\Delta H_f^q = \Delta H_f^{neutral} - q[\varepsilon(0/q)] + qE_F \quad (5)$$

where $\Delta H_f^{neutral}$ is the formation enthalpy of the neutral defect (eq 1) and E_F is the Fermi energy relative to the VBM of the stoichiometric host lattice; E_F is limited to the range between the VBM (0 eV) and the CBM (E_g). The ionization energy of the neutral defect to a charge state q, $\varepsilon(0/q)$, can be defined as the value of E_F for which $\Delta H_f^q = \Delta H_f^{neutral}$. $\varepsilon(0/q)$ is composed of two terms: the first accounts for the Coulomb and structural relaxation contributions, while the second accounts for the single electron defect level at the Γ point. Note that the calculated ionization energies are independent of the assumed chemical potentials.

$$\varepsilon(0/q) = \frac{[E^q_{Defect} - (E^{Neutral}_{Defect} - q\varepsilon^k_{Defect})] - q[\varepsilon^\Gamma_{Defect} - \varepsilon^\Gamma_{VBM(Host)}]}{-q} \quad (6)$$

By calculating $\varepsilon(0/q)$ in this way we are accounting for the unphysical dispersion of the defect levels in a supercell calculation with finite cell size, while maintaining precision in the total energies derived from more complete k-point sampling This becomes clearer in the rearrangement of $\varepsilon(0/q)$ in eq 7, where the correction term ($\varepsilon^k_{Defect} - \varepsilon^\Gamma_{Defect}$) tends toward zero as the dispersion of the defect band is reduced; the limit would be reached in an infinitely sized supercell.

$$\varepsilon(0/q) = \frac{E^q_{Defect} - E^{Neutral}_{Defect} + q[(\varepsilon^k_{Defect} - \varepsilon^\Gamma_{Defect}) + \varepsilon^\Gamma_{VBM(host)}]}{-q} \quad (7)$$

Here ε^k_{Defect} is the eigenvalue of the defect band averaged over each of the weighted k-points generated from a special

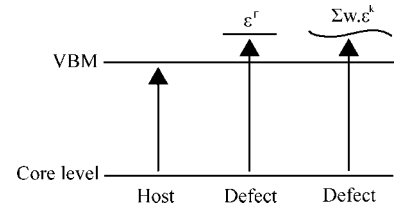

Figure 4. Illustration of the method used to determine defect levels in defective crystals relative to the valence band maximum (VBM) of the host crystal. ε^Γ is the eigenvalue of the defect at the gamma point, while w.ε^k is the weighted eigenvalue at each special k-point.

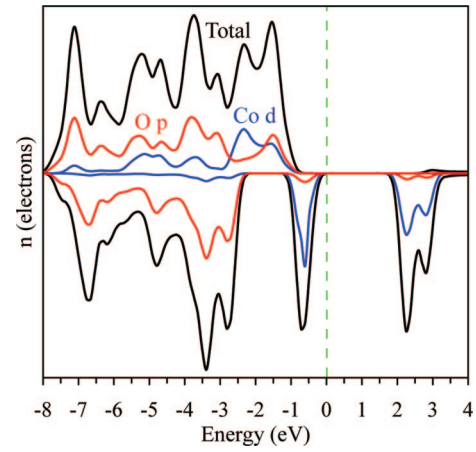

Figure 5. Calculated total and partial electronic density of states (DOS) of $CoAl_2O_4$. The top of the valence band is set to 0 eV, and the total DOS is ×2 for clarity.

Monkhorst−Pack grid.[33] $\varepsilon^\Gamma_{Defect}$ is the eigenvalue of the defect level determined at the zone center, while $\varepsilon^\Gamma_{VBM(host)}$ is the VBM of bulk $CoAl_2O_4$. Due to the arbitrary reference point of the Kohn−Sham eigenvalues, these levels are aligned relative to the energy of a 1s core level away from the defect center, as illustrated in Figure 4.

In a stoichiometric bulk insulator, the concentration of holes and electrons are equivalent, so the Fermi level will reside in the band gap center as the temperature tends to 0 K.[50] A consequence of eq 5 is that as the Fermi level is raised (with the increase in carrier electrons that occurs for n-type doping), the formation energy of ionized charge acceptors will be lowered; conversely, the formation energy of ionized charge donors is reduced as the Fermi level is lowered (with the increase in the concentration of holes that occurs for p-type doping). This imposes intrinsic limits on the generation of charge carriers within a material and forms the underpinning of the phenomenological doping limit rules for semiconductors.[44,51]

5. Self-Doping of $CoAl_2O_4$

The calculated electronic density of states (DOS) for bulk $CoAl_2O_4$ is shown in Figure 5. The valence band is spread over an 8 eV range consisting mainly of Co 3d and O 2p character. The majority spin e_g and t_{2g} Co 3d states are split between −6 and −1 eV, respectively, and show substantial hybridization with O 2p. The minority spin e_g states are also filled at the top of the valence band, with the bottom of the conduction band dominated by the minority spin t_{2g} states. It is therefore the Co 3d states that determine the fundamental band gap and in turn the redox characteristics of the material. The more ionic Al cation makes little contribution to the states in the valence band.

We have calculated seven intrinsic point defects in the $CoAl_2O_4$ lattice: V_{Co},V_{Al},O_i,V_O,Co_{Al}, Al_{Co},[Co_{Al}, Al_{Co}], where

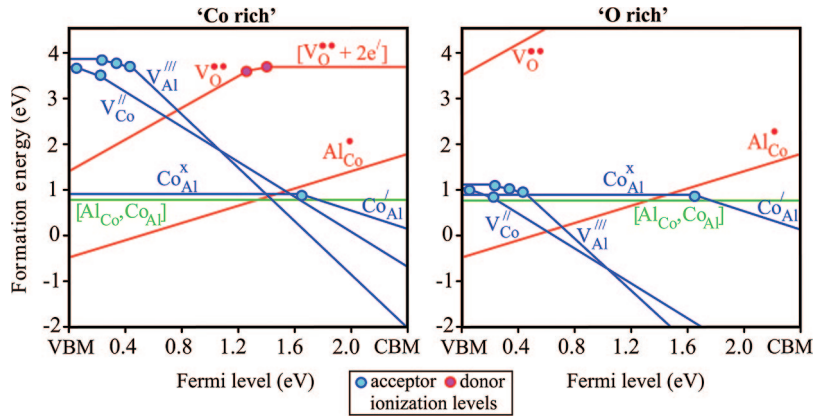

Figure 6. Calculated intrinsic defect formation energies as a function of the Fermi level (E_F) under Co rich ($\mu_{Co} = 0$ eV) and O rich ($\mu_O = 0$ eV) chemical potentials. The horizontal green line corresponds to the Co−Al site exchange.

TABLE 1: Calculated Defect Formation Enthalpies ($\Delta H_f^{neutral}$) in eV, under Cobalt ($\mu_{Co} = 0$ eV) and Oxygen ($\mu_O = 0$ eV) Rich Chemical Potentials

	$\Delta H_f^{neutral}$ (Co rich)	$\Delta H_f^{neutral}$ (O rich)
V_{Co}	3.84	1.01
V_{Al}	3.90	1.07
O_i	9.30	7.18
V_O	3.73	5.85
Co_{Al}	0.96	0.96
Al_{Co}	2.35	2.35
$[Co_{Al}, Al_{Co}]$	0.83	0.83
Fe_{Co}	0.77	0.82
Fe_{Al}	0.09	0.14

$[Co_{Al}, Al_{Co}]$ represents a site exchange between the Co and Al cations. Under Kröger−Vink notation,[50,52] both the neutral cell ($[V''_{Co} + 2h^{\bullet}]$, $[V'''_{Al} + 3h^{\bullet}]$, $[O''_i + 2h^{\bullet}]$, $[V^{\bullet\bullet}_O + 2e']$, Co_{Al}^{x}, $[Al^{\bullet}_{Co} + e']$) and charged cell (V''_{Co}, V'''_{Al}, O''_i, $V^{\bullet\bullet}_O$, Co'_{Al}, $Al^{\bullet}_{Co}$) defects were treated within the methodology described in the previous section. For example, an oxygen vacancy can be understood as generating two carrier electrons per defect center, $O_O \rightarrow [V^{\bullet\bullet}_O + 2e'] + 1/2O_2(g)$, while for the charge compensated cell these electrons are removed, i.e., $[V^{\bullet\bullet}_O + 2e'] \rightarrow [V^{\bullet\bullet}_O + e'] \rightarrow V^{\bullet\bullet}_O$. For a cation vacancy the situation is similar, with the generation of holes, $Co_{Co} \rightarrow [V''_{Co} + 2h^{\bullet}] + Co(s)$, which are removed for charge compensated calculations, i.e. $[V''_{Co} + 2h^{\bullet}] \rightarrow [V''_{Co} + h^{\bullet}] \rightarrow V''_{Co}$. The formation energy of each defect as a function of the Fermi level is shown in Figure 6 (and summarized in Table 1) under both equilibrium chemical potential conditions.

5.1. Formation of Acceptors Defects. Removal of either cation will result in a net electron deficiency and the generation of unoccupied acceptor levels within the band gap. Such empty defect bands situated close to the VBM (shallow acceptors) can be filled by thermal or optical excitation of valence electrons, resulting in the production of positive holes in the valence band (p-type carriers). Both V''_{Co} and V'''_{Al} are found to be reasonably shallow acceptors for oxides with ionization energies of 0.03 eV ($[V''_{Co} + 2h^{\bullet}] \rightarrow [V''_{Co} + h^{\bullet}]$) and 0.31 eV ($[V'''_{Al} + 3h^{\bullet}] \rightarrow [V'''_{Al} + 2h^{\bullet}]$), Figure 6. Unfortunately, under metal rich (oxygen poor) conditions, the formation energy of both defects is high, tending toward 4 eV as the Fermi level approaches the VBM. As V_{Al} becomes triply ionized (V'''_{Al}) above a Fermi energy of VBM + 0.4 eV, its formation energy is more sensitive to changes in the Fermi level than V''_{Co} due to the qE_F dependence in eq 7. A change to oxygen rich (metal poor) conditions reduces the cation chemical potentials, thus facilitating the removal of Al and Co from the system. The resulting formation energies tend toward an upper limit of 1.07 eV (1.01 eV) for V'''_{Al} (V''_{Co}) at the VBM, suggesting that under such conditions, both will be readily formed.

In $CoAl_2O_4$ each oxygen is coordinated to three Al cations and a single Co ion. For V''_{Co}, four oxygens lose their coordination to a Co(II) center, resulting in a nominal electron deficiency of 0.5 electrons per oxygen. For V'''_{Al}, six oxygens lose their coordination to an Al(III) center, which results in an equivalent charge deficit per ion. However, in both cases the unoccupied acceptor bands created in the band gap are of mixed Co 3d and O 2p character, as Co is more susceptible to further oxidation compared to Al. For V''_{Co}, the Al−O separations of the four perturbed oxygens contract by 0.09 Å relative to the equilibrium bond lengths, while for V'''_{Al} the Co−O (Al−O) distances contract by 0.12 (0.07) Å for the six perturbed oxygens.

The possibility of oxygen interstitial formation (O''_i) was investigated on both the available tetrahedral and octahedral sites, but their formation energy was found to be greater than 7 eV under all environments, due to repulsion from the underlying fcc oxygen sublattice in the spinel structure, Table 1. It is therefore unlikely that O''_i will be found in intrinsic $CoAl_2O_4$ samples.

5.2. Formation of Donor Defects. The creation of anion vacancies results in an excess of electrons and generally produces filled donor defect states in the band gap corresponding to reduced states of cationic character. If the defect band lies close to the CBM (shallow donor), the localized electrons can be readily ionized to the more dispersive conduction band (n-type carriers). For $CoAl_2O_4$, the formation of uncompensated oxygen vacancies ($[V^{\bullet\bullet}_O + 2e']$) is found to be high in energy (3.73 eV), even under metal rich conditions, Table 1. In an oxygen rich environment, the energetic cost of oxygen removal is increased to 5.85 eV indicating that few $V^{\bullet\bullet}_O$ will be present under such equilibrium conditions. In addition to the high formation energy, $V^{\bullet\bullet}_O$ produces a deep ($[V^{\bullet\bullet}_O + 2e'] \rightarrow [V^{\bullet\bullet}_O + e']$) donor level 0.9 eV below the CBM suggesting that even if formed, it would not generate a significant amount of mobile charge carriers. This is consistent with the concept that metal oxides with oxidizeable cations will not exhibit good n-type conduction.[50] Creation of an oxygen vacancy results in charge localization around the coordinated Co ion; the decreased oxidation states results in an expansion of the remaining three Co−O bond lengths of 0.08 Å, while the Al−O bond lengths remain relatively unperturbed, contracting by less than 0.02 Å.

We have also examined excess aluminum placed on a cobalt site. $Al^{\bullet}_{Co}$ produces a singly occupied donor state in the band gap corresponding to the difference in the +3 oxidation state

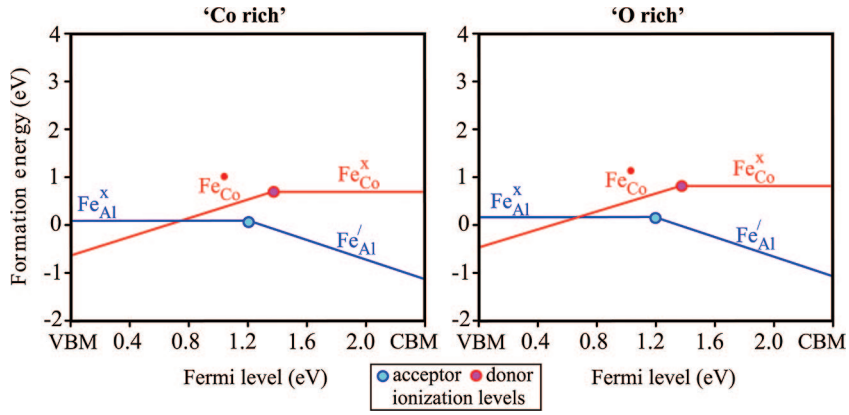

Figure 7. Calculated formation energies of Fe substitution as a function of the Fermi level (E_F) under Co rich ($\mu_{Fe} = -1.00$ eV) and O rich ($\mu_{Fe} = -3.88$ eV) chemical potentials.

of Al and the +2 oxidation state of the Co it replaces. The excess charge is distributed around each of the remaining Co ions. The calculated ($[Al^{\bullet}_{Co} + e'] \rightarrow Al^{\bullet}_{Co}$) transition state is found 0.1 eV above the CBM indicating that $Al^{\bullet}_{Co}$ is in fact stable across the accessible Fermi level range. Its low formation energy toward the VBM suggests that it is very likely to be present and contribute to partial charge compensation in the presence of excess positive holes.

5.3. Isovalent Defects. To investigate the effects of local cation site disorder we have treated a single site exchange between Co and Al, which is an electronically neutral defect. Interestingly for [Co_{Al}, Al_{Co}], Al maintains its characteristic +3 oxidation state, while Co is forced into a +2 oxidation state ($t_{2g}^{3\uparrow}t_{2g}^{3\downarrow}e_g^{1\uparrow}$) to preserve overall charge neutrality, i.e., [Co'_{Al}, $Al^{\bullet}_{Co}$]. A contraction of the Al−O interatomic distances from 1.94 to 1.83 Å occurs, consistent with the smaller ionic radius required to sustain an equivalent oxidation state in a lower coordination environment.[53] On the octahedral Co site, a change in coordination is also found. The $t_{2g}^{3\uparrow}t_{2g}^{3\downarrow}e_g^{1\uparrow}$ electronic configuration induces a local Jahn−Teller symmetry lowering from O_h to D_{4h}, with two 2.14 Å and four 2.00 Å Co−O bond lengths. This removes the degeneracy of the e_g levels, lowering the energy of the singly occupied d_{z^2} state. As local site disorder involves no change in system composition, the calculated formation energy of 0.83 eV is independent of the assumed chemical potential environment. While there are no surplus holes or electrons created, the presence of Co on the octahedral sites results in an almost 1 eV reduction in the band gap due to the filled $e_g^{\uparrow}$ state above the VBM.

As Co is stable in both +2 and +3 oxidization states, the substitution of excess cobalt on an aluminum site is also formally isovalent. Indeed the electronic configuration of neutral Co^{x}_{Al} is found to be low-spin d^6 ($t_{2g}^{3\uparrow}t_{2g}^{3\downarrow}$) with no local magnetic moment, isoelectronic to the octahedral Co sites in Co_3O_4. However, a deep unoccupied acceptor band with Co e_g character is found 1.7 eV above the VBM. Single occupation of this band results in a $t_{2g}^{3\uparrow}t_{2g}^{3\downarrow}e_g^{1\uparrow}$ configuration, i.e., a transition from Co(III) to Co(II) on the octahedral site ($Co^{x}_{Al} \rightarrow Co'_{Al}$). This d^7 electronic configuration is again stabilized through a local Jahn−Teller distortion. Under Co rich conditions, the formation energy of the neutral defect (Co^{x}_{Al}) is 0.96 eV. This implies that excess cobalt in the form of Co^{x}_{Al} is likely to be present to some degree under all equilibrium conditions.

6. Fe-Doping of $CoAl_2O_4$

The inclusion of Fe has been reported to increase the generated photocurrent relative to pure Co and Al spinels.[7] What is not clear is whether it is isolated doping of the host or the addition of new Fe-rich phases that improves photocurrent generation. To this end we investigated the substitution of Fe on both the Al and Co lattice sites, Figure 7. Due to the accessible +2 and +3 oxidation states of Fe, both Fe_{Co} and Fe_{Al} are formally isovalent substitutions.

6.1. Tetrahedral Fe Substitution. As expected for isolated substitution, Fe^{x}_{Co} adopts a d^6 electronic configuration with a high spin $e_g^{2\uparrow}t_{2g}^{3\uparrow}e_g^{1\downarrow}$ orientation characteristic of Fe(II). This produces a local magnetic moment of 3.6 μ_B. The Fe−O bond length relaxes from 1.98 Å R(Co−O) to 2.00 Å. A formation energy of 0.77 eV (0.82 eV) is found for Fe^{x}_{Co} under a metal rich (oxygen rich) environment. A filled deep level, localized on Fe, is formed in the minority spin channel ($e_g^{1\downarrow}$), 1 eV below the host CBM. Donation of this electron to the conduction band would correspond to an Fe(II) to Fe(III) transition on the tetrahedral site, or the loss of the minority spin e_g state ($Fe^{x}_{Co} \rightarrow Fe^{\bullet}_{Co}$).

6.2. Octahedral Fe Substitution. For Fe^{x}_{Al}, the O_h crystal field induces a high spin magnetic configuration of $t_{2g}^{3\uparrow}e_g^{2\uparrow}$ corresponding to a Fe(III) d^5 species, with a calculated local moment of 4.2 μ_B. The lowest energy is obtained when the magnetic spin is aligned antiferromagnetic relative to the tetrahedral Co sites, consistent with the ferrimagnetic behavior of Fe in Fe_3O_4 and Co_2FeO_4.[9] The formation energy of Fe^{x}_{Al} is lower than Fe^{x}_{Co}, varying between 0.09 and 0.14 eV within the chosen chemical potential range. This infers that Fe-doping of $CoAl_2O_4$ will produce Fe^{x}_{Al} in greater abundance, which is consistent with the only available neutron diffraction study of quaternary Co, Fe and Al spinels[54] that highlighted the presence of Fe on both the tetrahedral and octahedral sites, with a marked occupation of the octahedral positions. Here, converse to Fe^{x}_{Co}, there is a deep unoccupied acceptor level, localized on Fe, in the minority spin channel at 1.2 eV above the VBM. Occupation of this level would correspond to a Fe(III) to Fe(II) transition, or the addition of a minority spin $t_{2g}^{\downarrow}$ state ($Fe^{x}_{Al} \rightarrow Fe'_{Al}$).

7. Discussion

Details of the electronic properties and conductivity of $CoAl_2O_4$ in the literature are limited. A report of the electronic properties of stoichiometric $CoAl_2O_4$ from 1972 indicates weak p-type conductivity with thermal activation in the region of 0.8 eV, and a very sensitive temperature dependence indicative of small polaron conduction.[24] The correlated nature of the Co 3d states and covalent interactions between Co and O make it very susceptible to polaron hopping, which involves discrete jumps between localized states,[55] as opposed to typical semiconductor-

like free carrier conductivity through a delocalized valence or conduction band.

Under metal rich conditions the defect formation energies do not support free carrier p-type conduction, as the cost of creating shallow cation vacancy acceptors is too high. To this end, our results are consistent with the poor conductivity reported for $CoAl_2O_4$. However, the presence of Co_{Al}^{x}, which has a deep ($Co_{Al}^{'}$) acceptor level is likely, due to its lower formation energy. While free carriers will not be generated in any great abundance, polaron conductivity between the octahedral and tetrahedral Co sites mediated by the oxygen sublattice is possible.

Under oxygen rich conditions, very different behavior is implied from our results. The formation energy of the cation vacancies is lowered substantially, and both $V_{Co}^{''}$ and $V_{Al}^{'''}$ are relatively shallow acceptors suggesting that the electronic conductivity should rise significantly. Such a prediction is not completely unfounded: stoichiometric Co_3O_4 exhibits poor conductivity with a sensitive temperature dependence indicative of hopping polarons, while Co_3O_4 fabricated under metal poor conditions has recently been shown to result in a large increase in the number of Co vacancies and an exponential rise in conductivity.[56] We propose that a similar transition will be possible for $CoAl_2O_4$.

Local cation disorder has been shown to have a low barrier to formation, and can also contribute to a reduction of the electronic band gap. At the cation disorder limit (inverse spinel), the resulting band gap will be similar in magnitude to Co_2AlO_4, where Co atoms are randomly distributed over both the tetrahedral and octahedral sites.[9] This nonequilibrium structure is likely to have contributed to the low optical absorption onset ($\sim$1.7 eV) observed for the Co−Al spinels of Woodhouse et al.,[7,8] where less than ideal reaction temperatures were employed. This cation disorder is also the likely source of color changes observed in standard synthesis of $CoAl_2O_4$, where high temperature annealing over a long period is required to obtain blue crystals.

Isolated Fe substitution on both cation sites results in an isovalent ground-state electronic configuration with deep transition levels in the band gap corresponding to a Fe(II) $\leftrightarrow$ Fe(III) transition. As demonstrated by the high levels of polaron mediated conductivity exhibited by Fe_3O_4, and the lower II $\leftrightarrow$ III redox potential of Fe relative to Co,[57] the addition of Fe to $CoAl_2O_4$ should substantially aid polaron mobility. An analogous effect was observed in 1959 by Jonker[58] for Co_2FeO_4 where for Co rich compositions, polaron mobility is limited by Co ($E_{act} = 0.5$ eV), while for Fe rich compositions the activation energy is lowered ($E_{act} = 0.2$ eV) and the mobility is greatly increased. The high activation energy of 0.8 eV reported for $CoAl_2O_4$ suggests that even small amounts of Fe should produce a substantial effect in increasing polaron mobility. While isolated Fe defects are not expected to contribute significantly to the free carrier electronic conductivity, defect clusters and phase segregation could allow absorption of longer wavelength photons, contributing to increased photocurrent generation.

8. Conclusions

In conclusion, our examination of intrinsic defects and Fe-doping of $CoAl_2O_4$ indicates that oxygen rich (metal poor) conditions are required to make the formation of shallow acceptor cation vacancies energetically accessible, hence increasing the p-type semiconducting properties. Synthesis in such an environment should substantially increase the conductivity of $CoAl_2O_4$ over that reported for stoichiometric bulk samples in the literature. There is a low barrier to local Al and Co site disorder, and the presence of Co on the octahedral spinel sites results in a lowering of the electronic band gap, tending toward a 1 eV reduction for the fully inverse spinel. Fe readily substitutes for both Al and Co, but shows a stronger preference for the octahedral Al sites. However, Fe substitution generates no charge carriers, with a deep acceptor level corresponding to a Fe(III) to Fe(II) transition. While isolated Fe-doping may contribute to absorption of lower energy photons, it is not expected to greatly enhance the overall conductivity. The role of Fe-rich spinel phases and more complex defect configurations in improving absorption cannot be ruled out.

Acknowledgment. We thank M. Woodhouse and B. A. Parkinson for access to their detailed results. This work was supported by the U.S. Department of Energy through the UNLV foundation under Contract No. DE-AC36-99GO10337.

References and Notes

(1) Becquerel, E. *C. R. Acad. Sci. (Paris)* **1839**, *9*, 561.
(2) Becquerel, E. *C. R. Acad. Sci. (Paris)* **1839**, *9*, 145.
(3) Gratzel, M. *Nature* **2001**, *414*, 338.
(4) Rao, C. N. R.; Gopalakrishnan, J. *New Directions in Solid State Chemistry*; Cambridge University Press: Cambridge, 1997.
(5) Fujishima, A.; Kohayakawa, K.; Honda, K. *J. Electrochem. Soc.* **1975**, *122*, 1487.
(6) Fujishima, A.; Honda, K. *Bull. Chem. Soc. Jpn.* **1971**, *44*, 1148.
(7) Woodhouse, M.; Herman, G. S.; Parkinson, B. A. *Chem. Mater.* **2005**, *17*, 4318.
(8) Woodhouse, M.; Parkinson, B. A. *Chem. Mater.* **2008**, *20*, 2495.
(9) Walsh, A.; Wei, S.-H.; Yan, Y.; Al-Jassim, M. M.; Turner, J. A.; Woodhouse, M.; Parkinson, B. A. *Phys. Rev. B* **2007**, *76*, 165119.
(10) Alarcon, J.; Escribano, P.; Marin, R. M. *Br. Ceram. Trans. J.* **1985**, *84*, 170.
(11) Ji, L.; Tang, S.; Zeng, H. C.; Lin, J.; Tan, K. L. *Appl. Catal. A* **2001**, *207*, 247.
(12) Miller, A. *J. Appl. Phys.* **1959**, *30*, S24.
(13) Dunitz, J. D.; Orgel, L. E. *J. Phys. Chem. Solids* **1957**, *3*, 318.
(14) Segev, D.; Wei, S.-H. *Phys. Rev. B* **2005**, *71*, 125129.
(15) Wei, S.-H.; Zhang, S. B. *Phys. Rev. B* **2001**, *63*, 045112.
(16) Watson, G. W.; Willock, D. J. *Chem. Commun.* **2001**, 1076.
(17) Verwey, E. J. W.; Heilmann, E. L. *J. Chem. Phys.* **1947**, *15*, 174.
(18) Henderson, C. M. B.; Charnock, J. M.; Plant, D. A. *J. Phys.: Condens. Matter* **2007**, *19*, 076214.
(19) Wolska, E.; Catlow, C. R. A.; Piszora, P.; Woodley, S. M. *Comput. Chem. (Oxford)* **2000**, *24*, 603.
(20) Davies, M. J.; Parker, S. C.; Watson, G. W. *J. Mater. Chem.* **1994**, *4*, 813.
(21) Tielens, F.; Calatayud, M.; Franco, R.; Recio, J. M.; Perez-Ramirez, J.; Minot, C. *J. Phys. Chem. B* **2006**, *110*, 988.
(22) Tristan, N.; Hemberger, J.; Krimmel, A.; von Nidda, H. A. K.; Tsurkan, V.; Loidl, A. *Phys. Rev. B* **2005**, *72*, 174404.
(23) Suzuki, T.; Nagai, H.; Nohara, M.; Takagi, H. *J. Phys.: Condens. Matter* **2007**, *19*, 145265.
(24) Matveeva, N. G.; Shelykh, A. I. *Phys. Status Solidi B* **1972**, *50*, 83.
(25) Martinsons, A. *Electrode and Process for Making Same; Patent*, U. S., Ed.; PPG Industries: United States, 1973; *Vol. 3711397*.
(26) El Habra, N.; Crociani, L.; Sada, C.; Zanella, P.; Casarin, M.; Rossetto, G.; Carta, G.; Paolucci, G. *Chem. Mater.* **2007**, *19*, 3381.
(27) Zayat, M.; Levy, D. *Chem. Mater.* **2000**, *12*, 2763.
(28) Lavrenčič Štangar, U; Orel, B; Krajnc, M *J. Sol-Gel Sci. Technol.* **2003**, *26*, 771.
(29) Hohenberg, P.; Kohn, W. *Phys. Rev.* **1964**, *136*, B864.
(30) Kohn, W.; Sham, L. J. *Phys. Rev.* **1965**, *140*, A1133.
(31) Kresse, G.; Furthmüller, J. *Phys. Rev. B* **1996**, *54*, 11169.
(32) Kresse, G.; Furthmüller, J. *Comput. Mater. Sci.* **1996**, *6*, 15.
(33) Monkhorst, H. J.; Pack, J. D. *Phys. Rev. B* **1976**, *13*, 5188.
(34) Kresse, G.; Joubert, D. *Phys. Rev. B* **1999**, *59*, 1758.
(35) Blöchl, P. E. *Phys. Rev. B* **1994**, *50*, 17953.
(36) Anisimov, V. I.; Zaanen, J.; Andersen, O. K. *Phys. Rev. B* **1991**, *44*, 943.
(37) Dudarev, S. L.; Botton, G. A.; Savrasov, S. Y.; Humphreys, C. J.; Sutton, A. P. *Phys. Rev. B* **1998**, *57*, 1505.
(38) Perdew, J. P.; Burke, K.; Ernzerhof, M. *Phys. Rev. Lett.* **1996**, *77*, 3865.
(39) Janotti, A.; Van de Walle, C. G. *Phys. Rev. B* **2007**, *76*, 165202.

(40) Scanlon, D. O.; Walsh, A.; Morgan, B. J.; Nolan, M.; Fearon, J.; Watson, G. W. *J. Phys. Chem. C* **2007**, *111*, 7971.
(41) Morgan, B. J.; Watson, G. W. *Surf. Sci.* **2007**, *601*, 5034.
(42) Murnaghan, F. D. *PNAS* **1944**, *30*, 244.
(43) Furuhashi, H.; Inagaki, M.; Naka, S. *J. Inorg. Nucl. Chem.* **1973**, *35*, 3009.
(44) Wei, S.-H. *Comput. Mater. Sci.* **2004**, *30*, 337.
(45) Yan, Y.; Li, J. B.; Wei, S.-H.; Al-Jassim, M. M. *Phys. Rev. Lett.* **2007**, *98*, 135506.
(46) Yan, Y.; Al-Jassim, M. M.; Wei, S.-H. *Appl. Phys. Lett.* **2006**, *89*, 181912.
(47) Li, J.; Wei, S.-H.; Li, S. S.; Xia, J. B. *Phys. Rev. B* **2006**, *74*, 081201.
(48) Wei, S.-H; Zhang, S. B *J. Phys. Chem. Solids* **2005**, *66*, 1994.
(49) Dalpian, G. M; Wei, S.-H *J. Phys. Chem. Solids* **2005**, *66*, 2008.
(50) Smyth, D. M. *The Defect Chemistry of Metal Oxides*; Oxford University Press: Oxford, 2000.
(51) Zhang, S. B.; Wei, S.-H.; Zunger, A. *Phys. Rev. Lett.* **2000**, *84*, 1232.
(52) Kröger, F. A. *The Chemistry of Imperfect Crystals*; North-Holland: Amsterdam, 1974.
(53) Shannon, R. *Acta Crystallogr., Sect. A* **1976**, *32*, 751.
(54) Mostafa, F. M.; Ptasiewicz-Bak, H.; Ligenza, S. *Phys. Status Solidi A* **1985**, *91*, 99.
(55) Cox, P. A. *The Electronic Structure and Chemistry of Solids*; Oxford University Press: New York, 1987.
(56) Tronel, F.; Guerlou-Demourgues, L.; Menetrier, M.; Croguennec, L.; Goubault, L.; Bernard, P.; Delmas, C. *Chem. Mater.* **2006**, *18*, 5840.
(57) Lide, D. R. *CRC Handbook of Chemistry and Physics*, 88th ed.; CRC Press: Boca Raton, FL, 2007.
(58) Jonker, G. H. *J. Phys. Chem. Solids* **1959**, *9*, 165.

JP711566K